Relativistic mean-field study of neutron-rich nuclei

B. G. Todd* and J. Piekarewicz†
Department of Physics, Florida State University, Tallahassee, Florida 32306
(Received 28 January 2003; published 29 April 2003)

A relativistic mean-field model is used to study the ground-state properties of neutron-rich nuclei. Nonlinear isoscalar-isovector terms, unconstrained by present day phenomenology, are added to the model Lagrangian in order to modify the poorly known density dependence of the symmetry energy. These new terms soften the symmetry energy and reshape the theoretical neutron drip line without compromising the agreement with existing ground-state information. A strong correlation between the neutron radius of ^{208}Pb and the binding energy of valence orbitals is found: the smaller the neutron radius of ^{208}Pb, the weaker the binding energy of the last occupied neutron orbital. Thus, models with the softest symmetry energy are the first ones to drip neutrons. Further, in anticipation of the upcoming 1% measurement of the neutron radius of ^{208}Pb at the Thomas Jefferson Laboratory, a close relationship between the neutron radius of ^{208}Pb and neutron radii of elements of relevance to atomic parity-violating experiments is established.

DOI: 10.1103/PhysRevC.67.044317 PACS number(s): 21.10.Dr, 21.10.Gv

I. INTRODUCTION

Core-collapse supernovas and their remnant neutron stars are an important source of information pertaining to both superdense matter and nuclei far from the valley of stability. At present, however, important open questions remain in the understanding of the structure and dynamics of neutron stars, such as their size, composition, and cooling mechanism. Increased knowledge of these issues may in turn lead to a better understanding of stellar burning and heavy-element nucleosynthesis.

The structure of spherical neutron stars in hydrostatic equilibrium, the so-called Schwarszchild stars, is solely determined by the equation of state of neutron-rich matter in β equilibrium. Such an equation of state is well represented as the sum of two distinct components: (i) a symmetric ($N=Z$) component that is well constrained at saturation density plus (ii) a symmetry energy that accounts for any possible neutron-proton imbalance. Some of the important neutron-star properties mentioned above depend critically on the poorly known density dependence of the symmetry energy. Indeed, as a result of the saturation of symmetric nuclear matter, most of the pressure supporting the star up to about two times saturation density is provided by the symmetry energy.

In a set of recent papers, the sensitivity of the symmetry energy to changes in the model Lagrangian was investigated [1–4]. The model Lagrangian was modified by introducing nonlinear couplings between the isoscalar and the isovector mesons. These new terms enable one to modify the neutron skin of heavy nuclei without changing ground-state properties that are well constrained experimentally. It should be noted that precise information on the neutron radius of a heavy nucleus—^{208}Pb—might soon become available via a parity-violating electron scattering experiment at the Jefferson Laboratory that promises a 1% accuracy [6,5]. While such a measurement will provide the most accurate determination of the neutron density of a nucleus to date, it will also impact strongly on astrophysical observables. Indeed, a model-independent (or data-to-data) relation between the neutron skin of ^{208}Pb and the crust of a neutron star was recently established [1]. This strong correlation emerges as a result of the similar composition of the neutron skin of a heavy nucleus and the crust of a neutron star, namely, neutron-rich matter at similar densities. Further, the measurement of the neutron skin of ^{208}Pb constrains the cooling mechanism in neutron stars. A small neutron radius R_n suggests a soft symmetry energy which favors a small proton fraction in dense matter. In turn, a low proton concentration rules out the enhanced cooling of neutron stars via the direct URCA process [3]. If URCA cooling is indeed ruled out, then observations of enhanced cooling may provide strong evidence in support of exotic states of matter at the core of neutron stars (see, for example, Ref. [7]).

The density dependence of the symmetry energy should also play an important role on the properties of nuclei far from the valley of stability. Indeed, some theoretical calculations predict the emergence of new magic numbers as a result of a reduced spin-orbit splitting originating from a diffuse neutron skin [8,9]. This is most evident in the neutron-rich oxygen isotopes. The nucleus of ^{24}O, which in the traditional scheme has filled $1d^{5/2}$ and $2s^{1/2}$ orbitals, appears to be the heaviest member of the isotopic chain that remains stable against particle emission. Yet, most theoretical calculations predict the existence of the ''doubly magic'' nucleus ^{28}O. This issue continues to be revisited in light of a remarkable experiment that shows that the mere addition of a single proton stabilizes the fluorine chain up to ^{31}F; this is six more neutrons than in ^{24}O [10].

In this—our first—study of neutron-rich nuclei, we focus on the effect of the new isoscalar-isovector terms on ground-state properties. This study will be conducted within the framework of relativistic mean-field models that reproduce a large body of ground-state observables for nuclei at, or near, the valley of stability. Yet these observables are mostly insensitive to the density dependence of the symmetry energy.

*Email address: bonnie@godiva.physics.fsu.edu
†Email address: jorgep@csit.fsu.edu

It is the aim of the present study to constrain the symmetry energy through a systematic study of ground-state properties of neutron-rich nuclei. While we recognize that additional physics, such as pairing, may be needed for more realistic studies, we limit ourselves to study the impact of the bulk symmetry energy on the ground-state properties of neutron-rich nuclei. Further, we focus on self-consistent mean-field models in the hope of extending earlier studies of the linear response [11] to incorporate the new isoscalar-isovector terms.

The manuscript has been organized as follows. In Sec. II we review briefly the relativistic formalism paying special attention to the role of the new isoscalar-isovector couplings. We illustrate how these new couplings modify the density dependence of the symmetry energy while leaving unchanged all properties of symmetric nuclear matter. In Sec. III we present the results of the calculations for various ground-state observables for a variety of nuclei. A summary and conclusions are presented in Sec. IV.

II. FORMALISM

In this section, we describe in some detail the model Lagrangian employed in this work and the mean-field approximation used to compute ground-state properties for a variety of neutron-rich nuclei. Although most of the derivations are standard, a review is included here to illustrate the role of the mixed isoscalar-isovector meson terms first introduced in Ref. [1]. These terms, which supplement the phenomenologically successful Lagrangian of Ref. [12], modify the density dependence of the symmetry energy, thereby reshaping the nuclear landscape away from the valley of stability.

A. Effective Lagrangian

The Lagrangian of Ref. [12] includes an isodoublet nucleon field (ψ) interacting via the exchange of one scalar (ϕ for the sigma) and three vector (V^μ for the omega, $\mathbf{b}^\mu$ for the rho, and A^μ for the photon) fields. That is,

$$\begin{aligned}\mathcal{L}=\bar{\psi}\Big\{\gamma^\mu\Big(i\partial_\mu-g_{\rm v}V_\mu-\frac{g_\rho}{2}\boldsymbol{\tau}\cdot\mathbf{b}_\mu-\frac{e}{2}(1+\tau_3)A_\mu\Big)\\-(M-g_{\rm s}\phi)\Big\}\psi+\frac{1}{2}\partial^\mu\phi\,\partial_\mu\phi-\frac{1}{2}m_{\rm s}^2\phi^2-\frac{1}{4}V^{\mu\nu}V_{\mu\nu}\\+\frac{1}{2}m_{\rm v}^2V^\mu V_\mu-\frac{1}{4}\mathbf{b}^{\mu\nu}\cdot\mathbf{b}_{\mu\nu}+\frac{1}{2}m_\rho^2\,\mathbf{b}^\mu\cdot\mathbf{b}_\mu-\frac{1}{4}F^{\mu\nu}F_{\mu\nu}\\-U_{\rm eff}(\phi,V^\mu,\mathbf{b}^\mu),\end{aligned}\tag{1}$$

where the various field tensors have been defined as follows:

$$V_{\mu\nu}=\partial_\mu V_\nu-\partial_\nu V_\mu,\tag{2a}$$

$$\mathbf{b}_{\mu\nu}=\partial_\mu\mathbf{b}_\nu-\partial_\nu\mathbf{b}_\mu,\tag{2b}$$

$$F_{\mu\nu}=\partial_\mu A_\nu-\partial_\nu A_\mu.\tag{2c}$$

In addition to meson-mediated interactions, the Lagrangian is supplemented with nonlinear meson interactions that serve to simulate the complicated dynamics that lie beyond the realm of the low-energy effective theory. Indeed, by fitting the constants that parametrize these meson terms to the bulk properties of nuclei, rather than to two-nucleon data, the complicated dynamics originating from nucleon exchange, short-range effects, and many-body correlations get implicitly encoded in a small number of empirical constants. For the purpose of the present discussion, the following local meson terms are sufficient:

$$\begin{aligned}U_{\rm eff}(\phi,V^\mu,\mathbf{b}^\mu)=\frac{\kappa}{3!}\Phi^3+\frac{\lambda}{4!}\Phi^4-\frac{\zeta}{4!}(W_\mu W^\mu)^2\\-(\Lambda_{\rm s}\Phi^2+\Lambda_{\rm v}W_\mu W^\mu)(\mathbf{B}_\mu\cdot\mathbf{B}^\mu),\end{aligned}\tag{3}$$

where the following definitions have been introduced: $\Phi=g_{\rm s}\phi$, $W_\mu=g_{\rm v}V_\mu$, and $\mathbf{B}_\mu=g_\rho\mathbf{b}_\mu$. The inclusion of scalar-meson interactions (κ and λ) is dictated by the empirical value of the compression modulus of symmetric nuclear matter at saturation density ($K=200-300$ MeV). In contrast, quartic vector self-interactions (ζ) affect primarily the high-density component of the equation of state; their impact at densities below normal nuclear-matter saturation density is yet to be determined [12]. Finally, the nonlinear mixed isoscalar-isovector couplings ($\Lambda_{\rm s}$ and $\Lambda_{\rm v}$) are powerful terms because they can be used to modify the density dependence of the symmetry energy [1] while not influencing ground-state properties. While power counting suggests that other local meson terms (such as mixed scalar-vector cubic terms and quartic ρ-meson self-interactions) may be equally important [12], their phenomenological impact has been documented to be small [12,1], so they will not be considered in this study.

B. Mean-field equations

The field equations resulting from the above Lagrangian may be solved exactly in the mean-field limit by replacing all meson-field operators by their expectation values, which are classical fields [13]. For a static, spherically symmetric system this implies (using $|\mathbf{x}|\equiv r$)

$$\phi(x)\rightarrow\langle\phi(x)\rangle=\phi_0(r),\tag{4a}$$

$$V^\mu(x)\rightarrow\langle V^\mu(x)\rangle=g^{\mu0}V_0(r),\tag{4b}$$

$$b_a^\mu(x)\rightarrow\langle b_a^\mu(x)\rangle=g^{\mu0}\delta_{a3}\,b_0(r),\tag{4c}$$

$$A^\mu(x)\rightarrow\langle A^\mu(x)\rangle=g^{\mu0}A_0(r).\tag{4d}$$

Similarly, the various baryon sources to which these mesons couple must be replaced by their (normal-ordered) expectation values in the mean-field ground state. That is,

$$\bar{\psi}(x)\mathbf{1}\psi(x)\rightarrow\langle:\bar{\psi}(x)\mathbf{1}\psi(x):\rangle=\rho_{\rm s}(r),\tag{5a}$$

$$\bar{\psi}(x)\gamma^\mu\psi(x)\rightarrow\langle:\bar{\psi}(x)\gamma^\mu\psi(x):\rangle=g^{\mu0}\rho_{\rm v}(r),\tag{5b}$$

$$\bar{\psi}(x)\gamma^\mu\tau_a\psi(x)\rightarrow\langle:\bar{\psi}(x)\gamma^\mu\tau_a\psi(x):\rangle=g^{\mu0}\delta_{a3}\rho_3(r),\tag{5c}$$

$$\overline{\psi}(x)\gamma^{\mu}\tau_p\psi(x)\rightarrow\langle:\overline{\psi}(x)\gamma^{\mu}\tau_p\psi(x):\rangle=g^{\mu 0}\rho_p(r). \quad (5d)$$

Note that the proton isospin projection operator has been defined as $\tau_p=(1+\tau_3)/2$. The baryon sources generate (classical) meson fields that satisfy coupled, nonlinear Klein-Gordon equations of the following form:

$$\left(\frac{d^2}{dr^2}+\frac{2}{r}\frac{d}{dr}-m_{\rm s}^2\right)\Phi_0(r)-g_{\rm s}^2\left(\frac{\kappa}{2}\Phi_0^2(r)+\frac{\lambda}{6}\Phi_0^3(r)-2\Lambda_{\rm s}B_0^2(r)\Phi_0(r)\right)=-g_{\rm s}^2\rho_{\rm s}(r), \quad (6a)$$

$$\left(\frac{d^2}{dr^2}+\frac{2}{r}\frac{d}{dr}-m_{\rm v}^2\right)W_0(r)-g_{\rm v}^2\left(\frac{\zeta}{6}W_0^3(r)+2\Lambda_{\rm v}B_0^2(r)W_0(r)\right)=-g_{\rm v}^2\rho_{\rm v}(r), \quad (6b)$$

$$\left(\frac{d^2}{dr^2}+\frac{2}{r}\frac{d}{dr}-m_{\rho}^2\right)B_0(r)-2g_{\rho}^2[\Lambda_{\rm s}\Phi^2(r)+\Lambda_{\rm v}W_0^2(r)]B_0(r)=-\frac{g_{\rho}^2}{2}\rho_3(r). \quad (6c)$$

The photon field couples only to the (point) proton density and its solution is thus reduced to quadratures

$$A_0(r)=e\left[\frac{1}{r}\int_0^r dx\,x^2\rho_{\rm p}(x)+\int_r^{\infty}dx\,x\,\rho_{\rm p}(x)\right]. \quad (7)$$

The eigenstates of the Dirac equation, for the spherically symmetric mean-field ground state assumed here, may be classified according to a generalized angular momentum $\varkappa$. Thus, the single-particle solutions of the Dirac equation may be written as

$$\mathcal{U}_{n\varkappa mt}(\mathbf{x})=\frac{1}{r}\begin{pmatrix} g_{n\varkappa t}(r)\mathcal{Y}_{+\varkappa m}(\hat{\mathbf{x}}) \\ if_{n\varkappa t}(r)\mathcal{Y}_{-\varkappa m}(\hat{\mathbf{x}})\end{pmatrix}\zeta_t, \quad (8)$$

where ζ_t denotes a two-component (Pauli) spinor in isospin space (with $t=\pm 1/2$ for protons and neutrons, respectively), n and m are the principal and magnetic quantum numbers, respectively, and the spin-spherical harmonics are defined as

$$\mathcal{Y}_{\varkappa m}(\hat{\mathbf{x}})\equiv\left\langle\hat{\mathbf{x}}\middle|l\frac{1}{2}jm\right\rangle,\quad j=|\varkappa|-\frac{1}{2},\quad l=\begin{cases}\varkappa & \text{if } \varkappa>0\\ -1-\varkappa & \text{if } \varkappa<0.\end{cases} \quad (9)$$

Note that the phase convention adopted in Eq. (8) (i.e., the relative factor of (i) is such that real bound-state wave functions (g and f) are generated if the mean-field potentials are also real. Further, the following spinor normalization has been adopted:

$$\int d^3x\,\mathcal{U}_{\alpha}^{\dagger}(\mathbf{x})\mathcal{U}_{\alpha}(\mathbf{x})=\int_0^{\infty}dr\,[g_a^2(r)+f_a^2(r)]=1, \quad (10)$$

where $\{\alpha\}\equiv\{a=n\varkappa t;m\}$ denotes the collection of all quantum numbers required to describe the single-particle Dirac spinor. It then follows that the coupled differential equations satisfied by the radial components of the Dirac spinor are given by

$$\left(\frac{d}{dr}+\frac{\varkappa}{r}\right)g_a(r)-\left[E_a+M-\Phi_0(r)-W_0(r)\mp\frac{1}{2}B_0(r)-e\begin{Bmatrix}1\\0\end{Bmatrix}A_0(r)\right]f_a(r)=0, \quad (11a)$$

$$\left(\frac{d}{dr}-\frac{\varkappa}{r}\right)f_a(r)+\left[E_a-M+\Phi_0(r)-W_0(r)\mp\frac{1}{2}B_0(r)-e\begin{Bmatrix}1\\0\end{Bmatrix}A_0(r)\right]g_a(r)=0, \quad (11b)$$

where the upper and lower numbers in these equations correspond to protons and neutrons, respectively. Having determined all occupied single-particle states, the various ground-state densities, which act as sources for the meson fields in the Klein-Gordon equations [see Eq. (6)], may now be computed. They are given by

$$\rho_{\rm s}(r)=\rho_{\rm s,p}(r)+\rho_{\rm s,n}(r), \quad (12a)$$

$$\rho_{\rm v}(r)=\rho_{\rm v,p}(r)+\rho_{\rm v,n}(r), \quad (12b)$$

$$\rho_3(r)=\rho_{\rm v,p}(r)-\rho_{\rm v,n}(r), \quad (12c)$$

$$\rho_{\rm p}(r)=\rho_{\rm v,p}(r), \quad (12d)$$

where scalar and vector densities have been defined as

$$\begin{pmatrix}\rho_{\rm s,t}(r)\\ \rho_{\rm v,t}(r)\end{pmatrix}=\sum_{n\varkappa}^{\rm occ}\left(\frac{2j_{\varkappa}+1}{4\pi r^2}\right)[g_{n\varkappa t}^2(r)\mp f_{n\varkappa t}^2(r)]. \quad (13)$$

Ground-state properties of the system are described by a solution of the coupled, ordinary differential equations for the classical meson fields [Eq. (6)] and for the Dirac single-particle states [Eq. (11)]. The solution must be self-consistent, that is, the meson fields generating the Dirac mean-field potentials must satisfy Klein-Gordon equations having ground-state densities constructed from the same single-particle states as their sources. Thus, an iterative procedure must be implemented. The self-consistent procedure starts with initial Woods-Saxon shaped meson fields of reasonable strength and range to generate, via a conventional Runge-Kutta algorithm, bound-state energies and corresponding wave functions for all occupied single-particle states. At this point, scalar and vector densities ($\rho_{\rm s,t}$ and $\rho_{\rm v,t}$) are computed. Using these as sources for the meson-field equations, new meson fields are generated by using Green's function techniques. The newly generated meson fields will differ, in general, from the initial Woods-Saxon guess. Thus, this iterative procedure must continue until self-consistency (convergence) is achieved.

TABLE I. Model parameters used in the calculations. The parameter κ and the scalar mass m_s are given in MeV. The nucleon, ρ, and ω masses are kept fixed at $M=939$, $m_\rho=763$, and $m_\omega=783$ MeV, respectively—except in the case of the NL3 model where it is fixed at $m_\omega=782.5$ MeV.

Model	m_s	g_s^2	g_v^2	g_ρ^2	κ	λ	ζ
NL3	508.194	104.3871	165.5854	79.6000	3.8599	−0.01591	0.00
S271	505.000	81.1071	116.7655	85.4357	6.6834	−0.01580	0.00
Z271	465.000	49.4401	70.6689	90.2110	6.1696	+0.15634	0.06

III. RESULTS

The symmetry energy of infinite nuclear matter impacts on the dynamics of neutron-rich nuclei. After all, the symmetry energy describes how the energy of nuclear matter increases as the system departs from equal numbers of neutrons and protons. To investigate the structure of neutron-rich nuclei, we use a variety of effective field theory models that differ in their prediction for the density dependence of the symmetry energy.

Three models will be considered in this text: the very successful NL3 [14,15] along with the newer S271 and Z271 [1] parameter sets. The S271 and Z271 models are like the NL3 in that they are constrained to the following properties of symmetric nuclear matter: (i) nuclear saturation at a Fermi momentum of $k_F=1.30$ fm^{-1}, (ii) a binding energy per nucleon of 16.24 MeV, and (iii) a compression modulus of $K=271$ MeV. The first table (Table I) lists the various parameter sets that are needed to reproduce these properties of symmetric nuclear matter at the mean-field level.

In Fig. 1 the equation of state for symmetric nuclear matter is displayed for the three models discussed in the text. That all models are identical at (and near) saturation density follows from the fitting procedure that has produced the above mentioned constraints. While significant discrepancies among the models emerge at high density ($k_F \gtrsim 1.50$ fm^{-1}), presumably due to differences in the input values for the effective nucleon mass M^* and ζ, these discrepancies disappear at the densities ($k_F \lesssim 1.30$ fm^{-1}) relevant to the physics of finite nuclei (see inset in the figure). Thus, the equation of state for symmetric nuclear matter is model independent in this range and the only bulk property of infinite nuclear matter that can lead to a model dependence in ground-state observables of finite nuclei is the symmetry energy.

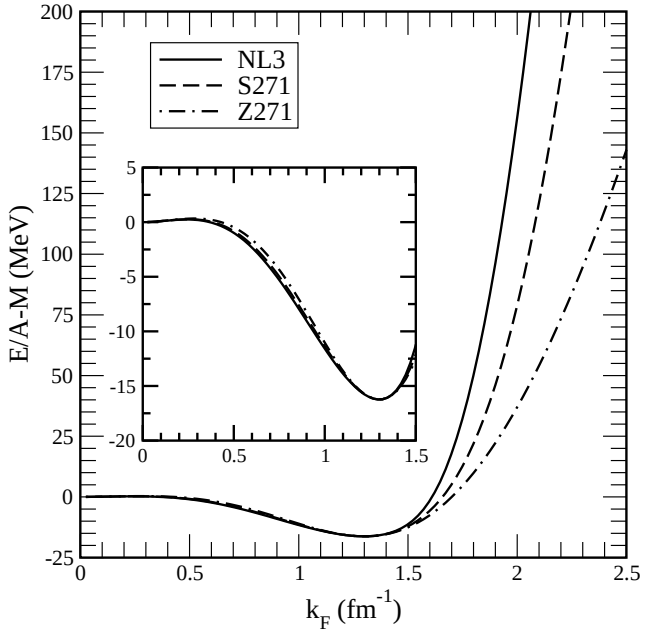

FIG. 1. Equation of state of symmetric nuclear matter for the three models considered in the text.

Unfortunately, the density dependence of the symmetry energy is poorly known. Indeed, even the symmetry energy at saturation density is not well constrained experimentally. It is some average between the symmetry energy at saturation density and the surface symmetry energy that is constrained by the binding energy of nuclei. As a consequence, we adjust the value of the $NN\rho$ coupling constant to reproduce a symmetry energy of $a_{\rm sym}=25.67$ MeV at a Fermi momentum of $k_F=1.15$ fm^{-1} (or $\rho=0.10$ fm^{-3}) [2,3]. (For a recent discussion on the surface symmetry energy see Ref. [16].)

In Table II predictions for the binding energy per nucleon [17], root-mean-square charge radius [18,19], and neutron radius of ^{208}Pb are displayed for the three models considered in the text. The predictions are within 1% of the experimental values, except for the neutron radius which is poorly known. The nonlinear coupling Λ_v between the isoscalar and the isovector mesons [see Eq. (3)] enables one to modify the density dependence of the symmetry energy, and thus the neutron radius of ^{208}Pb, while leaving well-known ground-state properties intact. This suggests that existing ground-state information, such as charge densities and binding energies, do not determine the neutron radius uniquely. Thus, a new measurement, such as the neutron radius in ^{208}Pb [6], is needed to provide important constraints on the density dependence of the symmetry energy. It is therefore the aim of

TABLE II. Symmetry energy at saturation density, binding energy per nucleon, root-mean-square charge radius (point-proton radius in parenthesis), and neutron radius of ^{208}Pb for the various models considered in the text (with $\Lambda_v=0$).

Model	$a_{\rm sym}^{\rm sat}$ (MeV)	B/A (MeV)	$R_{\rm ch}(R_p)$ (fm)	R_n (fm)
NL3	37.285	7.854	5.509 (5.460)	5.740
S271	36.637	7.939	5.509 (5.460)	5.714
Z271	36.298	7.775	5.508 (5.459)	5.700
Expt.	∼37	7.885	5.504	unknown

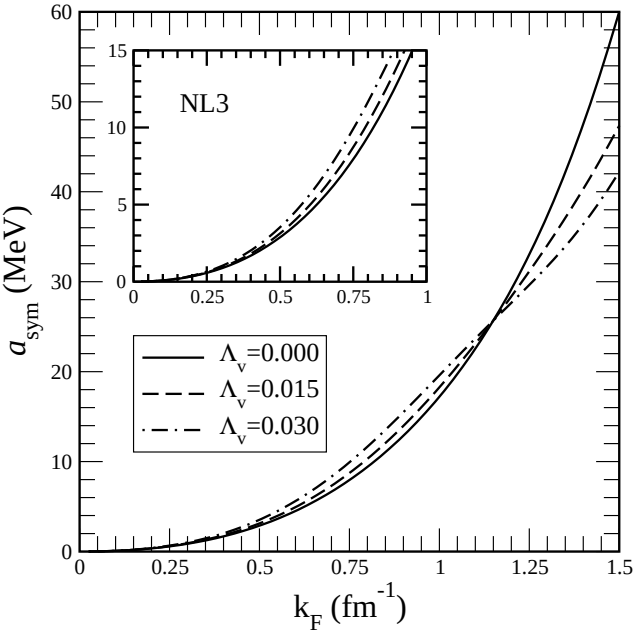

FIG. 2. The symmetry energy in the NL3 model.

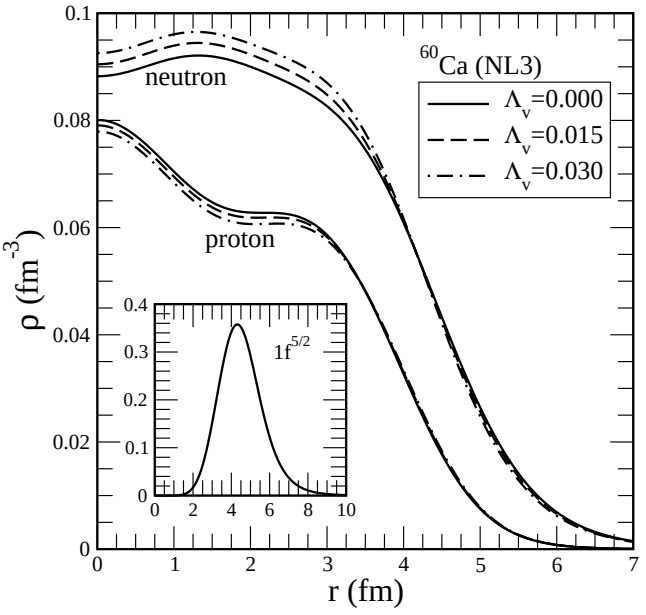

FIG. 3. Neutron and proton densities for ^{60}Ca in the NL3 model for various values of the isoscalar-isovector term Λ_v. The inset shows the surface-peaked nature of the (square of the) upper component of the least bound $1f^{5/2}$ neutron.

this paper to correlate ground-state properties of neutron-rich nuclei to the neutron radius of ^{208}Pb.

The model dependence of the symmetry energy is generated by tuning the isoscalar-isovector term. (For simplicity, we set the isoscalar-isovector coupling Λ_s to zero henceforth.) Note that changing Λ_v has no effect on the bulk properties of symmetric nuclear matter as the expectation value of the ρ-meson field is identically zero in the $N=Z$ limit. It does affect the value of the symmetry energy, so a mild adjustment of the $NN\rho$ coupling constant is required to keep the symmetry energy fixed at $a_{sym}=25.67$ MeV; this ensures that the binding energy per nucleon in ^{208}Pb remains fixed at 7.87 MeV [17].

In Fig. 2, the symmetry energy of infinite nuclear matter is plotted using the NL3 parameter set for different values of the isoscalar-isovector term Λ_v (the original NL3 parametrization has $\Lambda_v \equiv 0$ [14]). Increasing Λ_v softens the symmetry energy thereby reducing the internal pressure of the system. As a result, the original NL3 model predicts both the largest neutron radius in ^{208}Pb and the largest neutron-star radii (for a given mass) [1,2]. The inset in the figure shows the symmetry energy at the densities relevant to the dynamics of neutron-rich nuclei. Note that because all parametrizations are constrained to have the same symmetry energy at $k_F = 1.15$ fm^{-1}, models with a softer symmetry energy have a larger symmetry energy at low densities. In these softer models there is a higher price to pay for departing from equal numbers of protons and neutrons. This suggests a definite correlation: models with the smallest neutron skin ($R_n - R_p$) in ^{208}Pb should be the first ones to drip neutrons.

Further evidence for this behavior is provided in Fig. 3, where proton and neutron densities for the neutron-rich nucleus ^{60}Ca are displayed. The nonlinear isoscalar-isovector term Λ_v is used to change the density dependence of the symmetry energy which in turn modifies the neutron radius of $N \neq Z$ nuclei. Indeed, the predicted values for the neutron skin of ^{60}Ca are $R_n - R_p = 0.608, 0.567, 0.523$ fm for $\Lambda_v = 0, 0.015, 0.030$, respectively. Note that the proton radius remains fixed at $R_p = 3.562 \pm 0.013$ fm. The inset shows the square of the upper component of the least bound ($1f^{5/2}$) neutron in ^{60}Ca (for $\Lambda_v = 0$) to illustrate how it is most sensitive to the symmetry energy in the low-density surface region; this is the region (according to the inset in Fig. 2) where one expects the model with the largest neutron skin to give the strongest binding energy for the $1f^{5/2}$ neutron. In accordance with this statement we obtain a binding energy for the $1f^{5/2}$ neutron in ^{60}Ca of 4.907, 4.705, 4.443 MeV for a corresponding neutron skin of $R_n - R_p = 0.608, 0.567$, 0.523 fm, respectively.

This correlation is displayed in graphical form in the upper-left-hand panel of Fig. 4, where the binding energy of the least bound neutron in ^{60}Ca is plotted for the NL3 model (solid line) as a function of the neutron skin in ^{208}Pb. As evinced by the other panels in the figure, this correlation holds throughout the periodic table. Moreover, it is model independent. Indeed, similar plots have been added for the S271 (dashed line) and Z271 (dot-dashed line) parametrizations. In all cases the binding energy of the least bound neutron increases with increasing neutron skin. Note, however, that the shell ordering is not constrained among the models. For ^{60}Ca the NL3 model predicts the $1f^{5/2}$ orbital to be the least bound, whereas in the S271 and Z271 models it is the $2p^{1/2}$ orbital which is the least bound. Moreover, this correlation, namely, that an increase in the isoscalar-isovector coupling is responsible for a decrease in both the neutron skin of ^{208}Pb and in the binding energy of the least bound neutron of a nucleus, should only be applied within a model and should not be used to compare among different models.

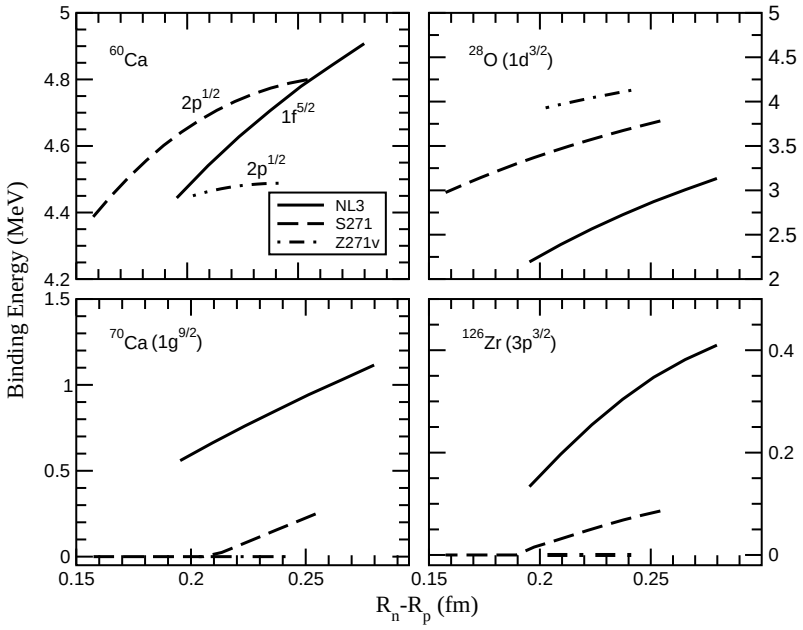

FIG. 4. The least bound neutron for various neutron-rich nuclei as a function of the neutron skin in ^{208}Pb for the three models considered in the text. A ''binding energy'' of 0 MeV indicates that the single-particle orbital is unbound.

Indeed, the Z271v model predicts the weakest (strongest) binding energy for the last neutron orbital in ^{60}Ca (^{28}O) among all the models.

A case of particular interest is the doubly magic nucleus ^{28}O (upper-right-hand panel of Fig. 4) which appears to be particle unstable [10] in spite of the many theoretical predictions to the contrary [20–23]. While the case of ^{28}O in particular, and the whole isotopic chain in general, deserves special attention and thus a separate publication, suffices to say that in all the self-consistent relativistic mean-field models considered here, the $1d^{3/2}$ orbital in ^{28}O is predicted to be bound by at least 2 MeV.

We finish the discussion of Fig. 4 by addressing the model dependence of the neutron drip lines in calcium and zirconium. Predictions for the least bound neutron in the neutron-rich nuclei ^{70}Ca (lower-left-hand panel) and ^{126}Zr (lower-right-hand panel) are displayed as a function of the neutron skin in ^{208}Pb. Note that a ''binding energy'' of 0 MeV indicates that the neutron is unbound and drips. The NL3 model predicts the last occupied neutron orbital in both nuclei ($1g^{9/2}$ and $3p^{3/2}$, respectively) to be bound, albeit only weakly. This is in contrast to the S271 model for which both single-particle orbitals are bound but only for those parametrizations with a large neutron skin in ^{208}Pb; that is, with a stiff symmetry energy. The Z271 model predicts both nuclei to be particle unstable for all values of $R_n - R_p$ in ^{208}Pb.

We conclude this section with a brief comment on the impact of a 1% measurement of the neutron radius in ^{208}Pb on the neutron radius of other heavy nuclei that have been identified as promising candidates for atomic parity-violation experiments: barium, dysprosium, and ytterbium [24–26]. Part of the appeal of these atoms is the existence of very close (nearly degenerate) levels of opposite parity that considerably enhance parity-violating amplitudes. Unfortunately, parity-violating matrix elements are contaminated by uncertainties in both atomic and nuclear structure. A fruitful experimental strategy for removing the sensitivity to the atomic theory is to measure ratios of parity-violation observables along an isotopic chain. This leaves nuclear-structure uncertainties, in the form of the neutron radius, as the limiting factor in the search for physics beyond the standard model [27–29]. All three elements, barium, dysprosium, and ytterbium, have long chains of naturally occurring isotopes. While the experimental strategy demands a precise knowledge of neutron radii along the complete isotopic chain, we only correlate here (as means of illustration) the neutron radius of ^{208}Pb to the neutron radius of a member of the isotopic chain having a closed neutron shell (or subshell); we only consider here: ^{138}Ba($Z=56;N=82$) [30], ^{158}Dy($Z=66;N=92$), and ^{176}Yb($Z=70;N=106$). Note that for the open proton shell a spherical average is performed. That is, the factor of $2j_k+1$ in Eq. (13) is simply replaced by the actual number of protons in the orbital.

The neutron skins of ^{138}Ba, ^{158}Dy, and ^{176}Yb, are correlated to the corresponding neutron skin of ^{208}Pb in the three panels of Fig. 5. We observe a tight linear correlation that is largely model independent. The linear regression coefficients (slope m and intercept b) have been enclosed in parenthesis. A theoretical spread of ≈ 0.3 fm in the neutron radius of ^{208}Pb was estimated in Refs. [27,31]. For two recent discussions on the extraction of the neutron skin of ^{208}Pb from proton-nucleus elastic scattering see Refs. [32,33]. Most of this spread is driven by the difference between relativistic and nonrelativistic models, which has recently been attributed to the poorly known density dependence of the symmetry energy [34]. With the culmination of the parity radius experiment at the Jefferson Laboratory [6], the theoretical spread will be replaced by a genuine experimental error that is five times smaller, that is, $\Delta R_n(^{208}\mathrm{Pb}) \simeq 0.056$ fm. This 1% measurement of the neutron radius in ^{208}Pb translates into a neutron radius uncertainty of $\Delta R_n(^{138}\mathrm{Ba}) \simeq 0.045$ fm, $\Delta R_n(^{158}\mathrm{Dy}) \simeq 0.034$ fm, and $\Delta R_n(^{176}\mathrm{Yb}) \simeq 0.052$ fm, respectively. While the model independence of these results is encouraging, one should test the proposed correlation be-

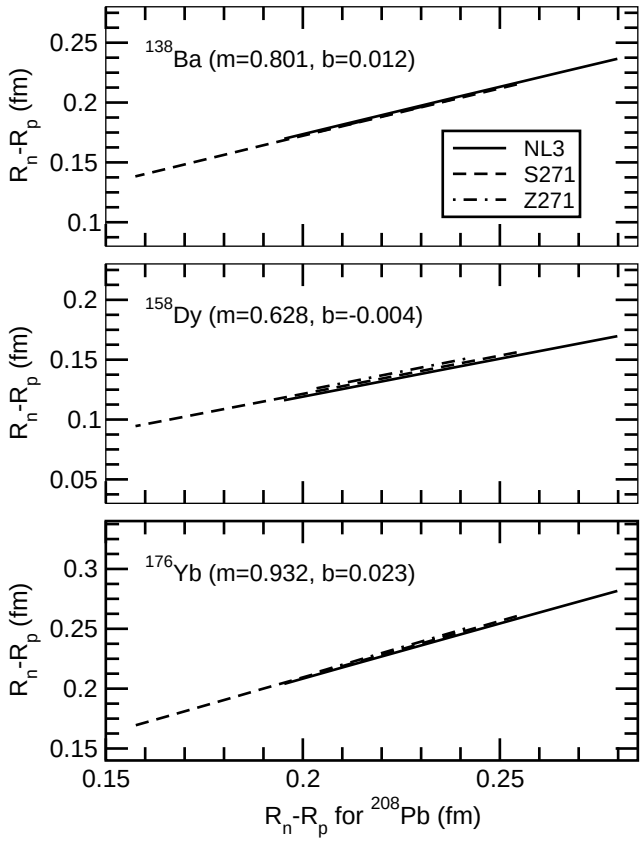

FIG. 5. Skin-skin correlations for three heavy nuclei of possible relevance to atomic parity violation (^{138}Ba, ^{158}Dy, and ^{176}Yb) as a function of the neutron skin of ^{208}Pb for the three models considered in the text. Quantities in parenthesis represent linear regression coefficients (slope and intercept).

tween the neutron radii of heavy nuclei in models that modify the density dependence of the symmetry energy in a manner that is different from the one presented here.

IV. CONCLUSIONS

The neutron radius of ^{208}Pb, an observable highly sensitive to the density dependence of the symmetry energy, is correlated to ground-state observables of neutron-rich nuclei. We find that models with small neutron skins in ^{208}Pb predict weak binding energies for the valence neutron orbitals in neutron-rich nuclei. Thus, models with the softest symmetry energy are the first ones to drip neutrons. Further, a tight correlation was found between the neutron skin of ^{208}Pb and the neutron radius of a variety of elements (barium, dysprosium, and ytterbium) of possible relevance to atomic parity violation.

The softening of the symmetry energy, which generates a thinner neutron skin in ^{208}Pb, is accomplished by introducing additional (isoscalar-isovector) terms into the effective Lagrangian. The new terms represent an important addition to the relativistic mean-field models, as they allow modifications to the neutron skin of ^{208}Pb without compromising their success in reproducing a variety of ground-state observables. At first, it might seem surprising that the neutron radius of ^{208}Pb, one of the most studied nuclei both theoretically and experimentally, should be so poorly known. Indeed, theoretical estimates place an uncertainty in the neutron radius of ^{208}Pb at about 0.3 fm. This is in contrast to its charge radius which is known—experimentally—to exquisite accuracy. The reason for this mismatch is twofold. First, electron scattering experiments, arguably the cleanest probe of nuclear structure, are only sensitive to the proton distribution. Second, best-fit models constrained to reproduce a variety of nuclear observables, such as charge densities, binding energies, and single-particle spectra, still predict a wide range of neutron radii for ^{208}Pb.

Fortunately, the measurement of the neutron radius of ^{208}Pb seems within reach. Indeed, the parity radius experiment at the Jefferson Laboratory aims to measure the neutron radius in ^{208}Pb accurately (at the 1% level) and model independently via parity-violating electron scattering. Such a measurement seems vital, as knowledge of a single isovector observable is sufficient to place stringent constraints on the model dependence of symmetry energy. Further, such a measurement will shed light on a variety of rich nuclear phenomena, ranging from the structure of neutron-rich nuclei to the structure of neutron stars.

ACKNOWLEDGMENTS

We thank Professor C.J. Horowitz for many useful discussions. This work was supported in part by U.S. DOE Grant No. DE-FG05-92ER40750.

[1] C.J. Horowitz and J. Piekarewicz, Phys. Rev. Lett. **86**, 5647 (2001).
[2] C.J. Horowitz and J. Piekarewicz, Phys. Rev. C **64**, 062802(R) (2001).
[3] C.J. Horowitz and J. Piekarewicz, Phys. Rev. C **66**, 055803 (2002).
[4] J. Carriere, C.J. Horowitz, and J. Piekarewicz, nucl-th/0211015.
[5] C.J. Horowitz, S.J. Pollock, P.A. Souder, and R. Michaels, Phys. Rev. C **63**, 025501 (2001).
[6] R. Michaels, P.A. Souder, and G.M. Urciuoli, spokespersons, Jefferson Laboratory Experiment E-00-003.
[7] P. Slane, D.J. Helfund, and S.S. Murray, Astrophys. J. Lett. **571**, L45 (2002).
[8] J. Dobaczewski, I. Hamamoto, W. Nazarewicz, and J.A. Sheikh, Phys. Rev. Lett. **72**, 981 (1994).
[9] T. Otsuka, R. Fujimoto, Y. Utsuno, B.A. Brown, M. Honma, and T. Mizusaki, Phys. Rev. Lett. **87**, 082502 (2001).
[10] H. Sakurai *et al.*, Phys. Lett. B **448**, 180 (1999).
[11] J. Piekarewicz, Phys. Rev. C **62**, 051304(R) (2000); **64**, 024307 (2001).
[12] H. Müller and B.D. Serot, Nucl. Phys. **A606**, 508 (1996).
[13] B.D. Serot and J.D. Walecka, Adv. Nucl. Phys. **16**, 1 (1986); Int. J. Mod. Phys. E **6**, 515 (1997).

[14] G.A. Lalazissis, J. König, and P. Ring, Phys. Rev. C **55**, 540 (1997).
[15] G.A. Lalazissis, S. Raman, and P. Ring, At. Data Nucl. Data Tables **71**, 1 (1999).
[16] Pawel Danielewicz, nucl-th/0301050.
[17] G. Audi and A.H. Wapstra, Nucl. Phys. **A595**, 409 (1995).
[18] H. de Vries, C.W. de Jager, and C. De Vries, At. Data Nucl. Data Tables **36**, 495 (1987).
[19] G. Fricke, C. Bernhardt, K. Heilig, L.A. Schaller, L. Schellenberg, E.B. Shera, and C.W. Dejager, At. Data Nucl. Data Tables **60**, 177 (1995).
[20] E.K. Warburton, J.A. Becker, and B.A. Brown, Phys. Rev. C **41**, 1147 (1990).
[21] Zhongzhou Ren, W. Mittig, Baoqiu Chen, and Zhongyu Ma, Phys. Rev. C **52**, R20 (1995).
[22] A.T. Kruppa, P.-H. Heenen, H. Flocard, and R.J. Liotta, Phys. Rev. Lett. **79**, 2217 (1997).
[23] G.A. Lalazissis, D. Vretanar, W. Pöschl, and P. Ring, Nucl. Phys. **A632**, 363 (1998).
[24] Xiong Xiaxing, He Mouqi, Zhao Youyuan, and Zhang Zhiming, J. Phys. B **23**, 4239 (1990); **23**, 4239 (1991).
[25] David DeMille, Phys. Rev. Lett. **74**, 4165 (1995).
[26] D. Budker, in *Proceedings of WEIN-98*, edited by P. Herczeg, C.M. Hoffman, and H.V. Klapdor-Kleingrothaus (World Scientific, Singapore, 1999).
[27] S.J. Pollock, E.N. Fortson, and L. Wilets, Phys. Rev. C **46**, 2587 (1992).
[28] B.Q. Chen and P. Vogel, Phys. Rev. C **48**, 1392 (1993).
[29] M.J. Ramsey-Musolf, Phys. Rev. C **60**, 015501 (1999).
[30] S. Schramm, nucl-th/0210053.
[31] R.J. Furnstahl, Nucl. Phys. **A706**, 85 (2002).
[32] S. Karataglidis, K. Amos, B.A. Brown, and P.K. Deb, Phys. Rev. C **65**, 044306 (2002).
[33] B.C. Clark, L.J. Kerr, and S. Hama, nucl-th/0209052.
[34] J. Piekarewicz, Phys. Rev. C **66**, 034305 (2002).